Ocean Engineering 343 (2026) 123432

Contents lists available at ScienceDirect

Ocean Engineering

journal homepage: www.elsevier.com/locate/oceaneng

Research paper

Consolidated combined V-H-M-T capacity of a suction caisson in clay

Hao Ran Li [a], Xiu Zhe Wang [b], Jiang Tao Yi [a,*], Hong Yu Tang [a], Xiao Han [a]

[a] School of Civil Engineering, Chongqing University, No.83 Shabei Street, Chongqing, 400045, China
[b] Faculty of Civil Engineering and Geoscience, Delft University of Technology, Stevinweg 1, Delft, 2628CN, the Netherlands

ARTICLE INFO

Keywords:
Suction caisson
Consolidation
Combined loading
Bearing capacity
Preload
Clay

ABSTRACT

Suction caissons are widely used as foundations for fixed wind turbines, floating wind systems, and subsea manifold systems due to their robust capacity to withstand environmental loads. Although the effect of torsion on the bearing capacity of suction caisson has been extensively studied, the influence of consolidation has not been adequately considered, despite its potential to enhance capacity and serve as a viable method to mitigate the reduction caused by torsional loading. This paper investigates the bearing capacity of suction caissons under combined V-H-M-T loading and the influence of consolidation on the failure envelope through coupled small-strain finite element analyses. A series of expressions for failure envelopes are proposed, and a generalized method is introduced to predict the consolidated failure envelope for any degree of preloading and consolidation.

1. Introduction

Suction caissons are steel, open-bottomed bucket foundations that are initially penetrated into the seabed under self-weight, forming a sealed chamber. Subsequent pumping of water from the interior creates a pressure differential between the inside and outside of the caisson, enabling full penetration. Owing to its simple and rapid installation process, as well as its robust capacity to withstand complex environmental loads, suction caissons have been extensively adopted in various aspects of offshore engineering. For fixed wind turbines in shallow water, they may serve as an independent foundation or be deployed in groups to support tripod or jacket substructures. In deep-water floating wind turbine systems, suction caissons act as anchoring systems to maintain station-keeping (Andersen et al., 2005; Randolph et al., 2011). Within the oil and gas industry, they are employed in manifold systems to support wellheads or pipeline terminals (Bughi and Parker, 2011). Recently, a novel concept has been proposed in which suction caissons could function as shared anchor points within offshore wind farms, simultaneously mooring multiple floating turbines (Gaudin et al., 2018; Herduin et al., 2018).

A substantial body of existing research has focused on the bearing capacity of suction caissons under combined VHM loading (Bransby and Randolph, 1998; Bransby and Yun, 2009; Alimoradi et al., 2024; Suryasentana et al., 2024). However, as the applications of suction caissons continue to diversify, the foundation may be subjected to more complex environmental loads. For instance, suction caissons serving as manifold foundations may experience non-planar forces transferred from the superstructure (Nouri et al., 2014); mooring line tensions applied to suction anchors may introduce load inclinations of approximately 5° (Fu et al., 2021); and misalignment during installation (Newlin, 2012), can induce significant torsional loading on suction caissons. These observations highlight the need for further investigation into the torsional bearing capacity, which may become a critical factor govern the failure of foundation.

Saviano and Pisanò (2017) examined the influence of installation-induced misalignment torque on the VH bearing capacity envelope of suction caissons and established a relationship between the misalignment angle and the subsequent contraction of the envelope. Fu et al. (2021) developed a modified suction caisson equipped with anti-rotational fins and systematically evaluated the resulting enhancement in torsional capacity. Chen et al. (2023) investigated the undrained combined bearing capacity of caissons with aspect ratios up to 1 under fully three-dimensional loading conditions across various soil profiles. Liu et al. (2023) extended this work to higher aspect ratios ($L/D = 1 - 2$), exploring the failure envelopes under combined VHM loading and specifically assessing the effect of torsion on the shape and size of the VHM capacity surface.

Existing research outputs consistently indicate that the application of torsional loading reduces the bearing capacity of foundations, underscoring the necessity of accounting for torsion during the design phase.

* Corresponding author.
E-mail addresses: Izzy-Lee@outlook.com (H.R. Li), X.Z.Wang@tudelft.nl (X.Z. Wang), yijt@foxmail.com (J.T. Yi), 20221601027@stu.cqu.edu.cn (H.Y. Tang), hanxiao@stu.cqu.edu.cn (X. Han).

https://doi.org/10.1016/j.oceaneng.2025.123432
Received 18 September 2025; Received in revised form 2 November 2025; Accepted 2 November 2025
Available online 7 November 2025

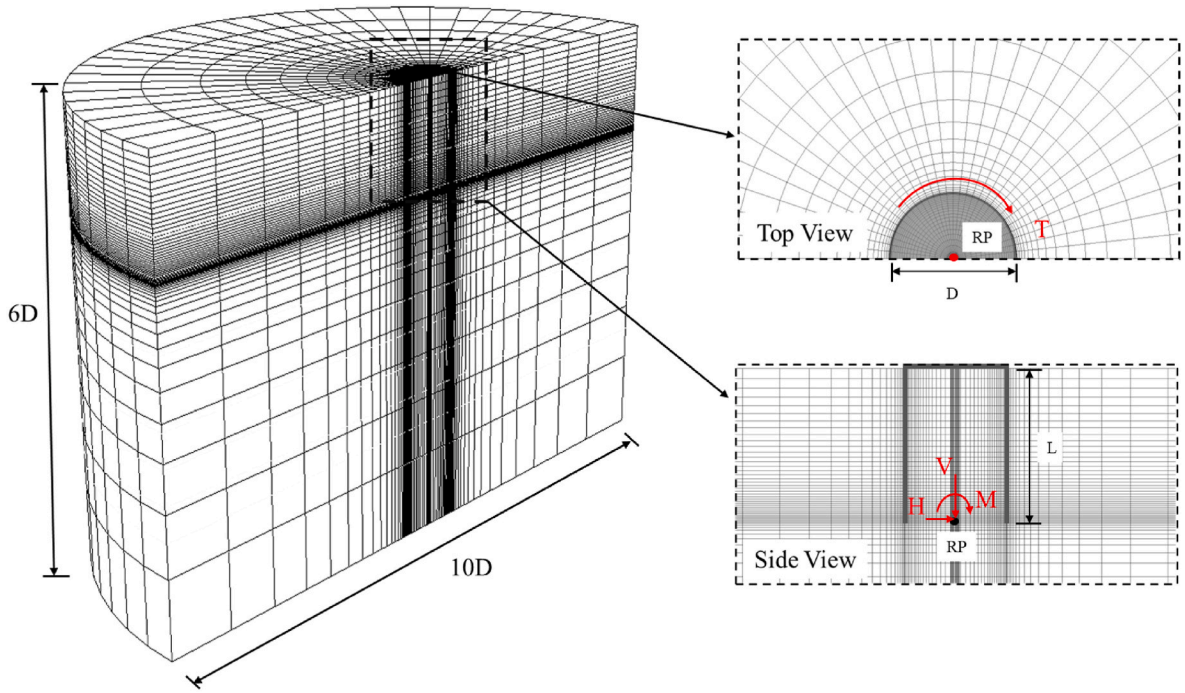

Fig. 1. Half-view of the finite element mesh for suction caisson.

Conventional design practices typically compare the foundation's capacity with the worst-case loading conditions to determine its geometry and size, yet often overlook the beneficial effects of consolidation, which can enhance the foundation bearing capacity. In offshore engineering, a period of several months may elapse between foundation installation and operational service. During this time, the soil beneath the foundation undergoes consolidation under the self-weight of the foundation and superstructure, leading to an increase in soil strength and consequently improved foundation capacity. Beyond passive preloading under self-weight, active preloading methods, such as ballasting or applying suction at the foundation base, can also be employed to provide additional safety margins (Randolph and Gourvenec, 2011). Bransby (2002) investigated the undrained inclined load capacity of surface strip foundations after preloading and consolidation, proposing a work-hardening law that relates capacity enhancement to consolidation settlement. Gourvenec et al. (2014) extended this framework by introducing a simplified method using critical state soil mechanics to predict the consolidated undrained bearing capacity of shallow foundations on soils with varying over-consolidation ratios (OCR), expressed as a function of preload magnitude and duration. Feng and Gourvenec (2015) applied this approach to study the consolidated failure envelope of rectangular surface foundations under combined loading in six degrees of freedom and observed that the expanded failure envelope post-consolidation maintains a shape similar to the unconsolidated envelope. Vulpe et al. (2016) examined the influence of aspect ratio on the consolidated failure envelope of skirted circular foundations and introduced a new scaling factor incorporating aspect ratio to accurately predict the capacity under various geometries. Fu et al. (2018) explored the effects of preload degree and consolidation time on the combined capacity of a caisson foundation with an aspect ratio of 0.2 under different soil heterogeneity conditions, noting that heterogeneity significantly influences the shape of the consolidated envelope.

Despite these advances, the consolidated failure envelope of suction caissons under combined loading including torsion has received limited attention, even though it may improve overall capacity and counteract the reduction induced by torsion. Incorporating consolidation effects resulting from self-weight or preloading into design not only provides additional safety margin for extreme loading but may also allow foundation size optimization based on environmental conditions, both of significant interest in offshore engineering.

This study conducted a series of three-dimensional coupled small-strain finite element analyses to investigate the expanded failure envelope of a suction caisson in normally consolidated clay after consolidation. With using the theoretical framework of critical state soil mechanics, the increase in undrained uniaxial capacities post-consolidation is predicted, and a method is proposed to estimate the consolidated failure envelope as a function of preload degree and consolidation duration.

2. Numerical analysis

All the three-dimensional small strain analyses are carried out on commercial code Abaqus (Dassault Systèmes, 2014).

2.1. Finite element model

In this study, a full soil domain model was adopted to account for the effect of torsional loading. Half of the finite element mesh is illustrated in Fig. 1. Given that suction caissons used as foundations for pipeline systems in deep-water oilfields typically exhibit aspect ratios between 1 and 2 (Liu et al., 2023), an impermeable rigid suction caisson with a skirt length $L = 15$ m and diameter $D = 10$ m was considered, resulting in an aspect ratio of 1.5. The skirt thickness t_w was set to 0.05 m for all analyses, yielding a diameter-to-thickness ratio D/t_w of 200, which falls within the typical range for in-situ steel suction caissons ($D/t_w = 100 - 500$) (Bye et al., 1995; Zhang et al., 2024). The reference point (RP) was defined at the midpoint of the foundation skirt tip level, where both preload and displacements were applied (Fig. 1).

The soil domain extended 10D in diameter and 6D in depth, dimensions sufficiently large to minimize boundary effects (Hung and Kim, 2012). The soil was discretized using first-order full integration stress–pore fluid continuum elements (C3D8P in Abaqus/Standard). A refined mesh with a minimum element size of 0.01D was employed around the foundation, transitioning gradually to coarser elements in remote regions to balance computational accuracy and efficiency. The top surface of the soil was assigned as a permeable drainage boundary to

Table 1
Soil parameters of Malaysian kaolin clay.

Parameters	Value
Slope of critical state line (CSL) in $p' - q$ space, M_{cs}	0.9
Critical friction angle in triaxial compression, φ'	23°
Saturated bulk unit weight, γ_{sat}	16.0 kN/m^3
Poisson ratio, υ	0.3
Permeability of soil, k	1.3×10^{-9} m/s
Virgin compression index, λ	0.205
Swelling and recompression index, κ	0.044
Void ratio at $p' = 1$ kPa on virgin consolidation line (VCL), e_N	2.252

allow dissipation of excess pore pressure during consolidation. All external boundaries were constrained in their normal directions. The soil–foundation interface was modeled as fully bonded, leading to rough in shear and no detachment permitted.

2.2. Soil properties

The numerical analyses were performed using the Modified Cam-Clay (MCC) soil model implemented in Abaqus. The soil parameters are adopted from the elemental tests of kaolin clay (Steward, 1992) (Table 1). The soil was considered to be K_0 consolidated with $K_0 = 1 - sin\,\varphi = 0.61$. The initial void ratio e_0 can be described by:

$$e_0 = e_N - \kappa\, ln\, p_0' - (\lambda - \kappa) ln\, p_{c0}' \tag{1}$$

where p_0' is the initial mean normal effective stress, p_{c0}' is the initial pre-consolidation pressure. Then the initial coefficient of consolidation c_{v0} can be expressed as:

$$c_{v0} = \frac{k(1+e_0)p_0'}{\lambda \gamma_w} \tag{2}$$

where γ_w is the unit weight of water, the undrained shear strength profile can be deduced from the MCC parameters as (Wroth, 1984):

$$\frac{s_u}{\sigma_v'} = \frac{M_{cs}\cos\theta}{\sqrt{3}} \left(\frac{p_{c0}'}{2p_0'}\right)^{\frac{\lambda-\kappa}{\lambda}} \frac{1+2K_0}{3} \tag{3}$$

where θ is Lode's angle, taken as – 30° for triaxial compression conditions.

2.3. Analysis procedure

Prior to consolidation analysis, the foundation was first subjected to vertical displacement-controlled loading until failure to determine its undrained unconsolidated bearing capacity V_u. Subsequently, a pre-defined fraction of V_u was applied as a preload V_p to the foundation. Following preloading, the foundation was maintained under constant load while excess pore pressure dissipation was permitted until the target degree of consolidation was achieved. Upon completion of consolidation, displacement-controlled loading was applied to the foundation to determine its consolidated uniaxial capacities.

The combined bearing capacity is evaluated using either the side-swipe test or the constant-ratio displacement-controlled probe test. The sideswipe test can determine the capacity surface in the VH, VM, or VT plane within a single analysis. In this method, the foundation is first loaded under vertical displacement until it reaches its vertical bearing capacity. Subsequently, while maintaining the vertical displacement constant, horizontal displacement or rotation is applied (Tan, 1990). The sideswipe test is stably implemented in Abaqus and does not require pre-calculation and setting of displacement increments for multiple discrete stages, as in the sequential swipe test. Moreover, according to Suryasentana et al. (2020) and Fan et al. (2023), the time required for the sequential swipe test is significantly longer than that for the side-swipe test. In Suryasentana's study, all calculations for a caisson foundation took only 23 h using the sideswipe test, whereas the sequential swipe test required 59.5 h, that is nearly three times longer. In Fan's study, a single calculation for a caisson foundation took only 21.5 min with the sideswipe test, while the sequential swipe test required at least 144.8 min. Therefore, for the extensive finite element cases in this paper, the sideswipe test is the most efficient method while ensuring computational accuracy. Capacity surfaces in other planes are tracked using the constant-ratio displacement-controlled probe test. Each analysis with a fixed displacement ratio can identify only one point on the capacity surface, therefore, multiple analyses are typically required to fully define the complete capacity surface within a given plane (Bransby and Randolph, 1998; Gourvenec and Randolph, 2003).

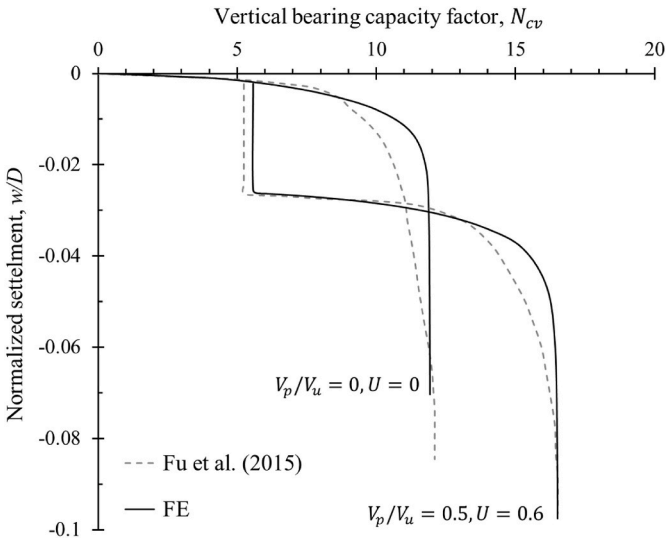

Fig. 2. Comparison of finite element results and centrifuge measurements on the post-consolidation bearing capacity factor N_{cv}

3. Validation

Since obtaining the consolidated failure envelope of suction caissons requires ensuring the accuracy of both the uniaxial capacities before and after consolidation, as well as the unconsolidated combined bearing capacity envelope, this section validates the uniaxial and combined capacities obtained in this study through comparisons with existing research results.

3.1. Uniaxial capacity

To validate the accuracy of the uniaxial capacity of the suction caisson, the consolidated uniaxial capacity analyses was conducted to replicate the centrifuge test of a preloaded skirted foundation by Fu et al. (2015). In the centrifuge test a preloaded skirted foundation was penetrated in UWA kaolin clay at various preload V_p with different consolidation time t_c to investigate the gain in bearing capacity after preloading and consolidation. A circular skirted foundation with a diameter of 70 mm and skirt length of 14 mm was first embedded into the soil under 1g acceleration. Subsequently, load-controlled loading at 200g acceleration was applied to achieve the target preload V_p, which was maintained for a specified consolidation period t. Upon reaching the predetermined consolidation degree U, displacement-controlled penetration was implemented until a failure state was attained. Fig. 2 shows the bearing capacity factor ($N_{cv} = V/As_{u0}$, A is the cross-sectional area of the foundation, s_{u0} is the undrained shear strength at the skirt tip level) of the skirted foundation under two conditions: no preload no consolidation and 0.5 times ultimate bearing capacity preload with 0.6 consolidation degree. The numerical results show good agreement with the centrifuge tests.

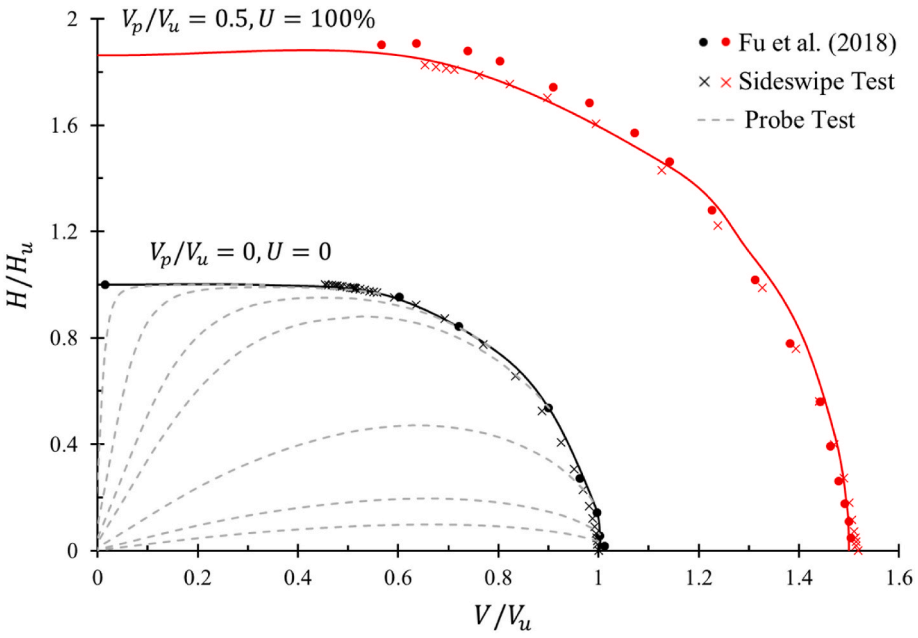

(a)

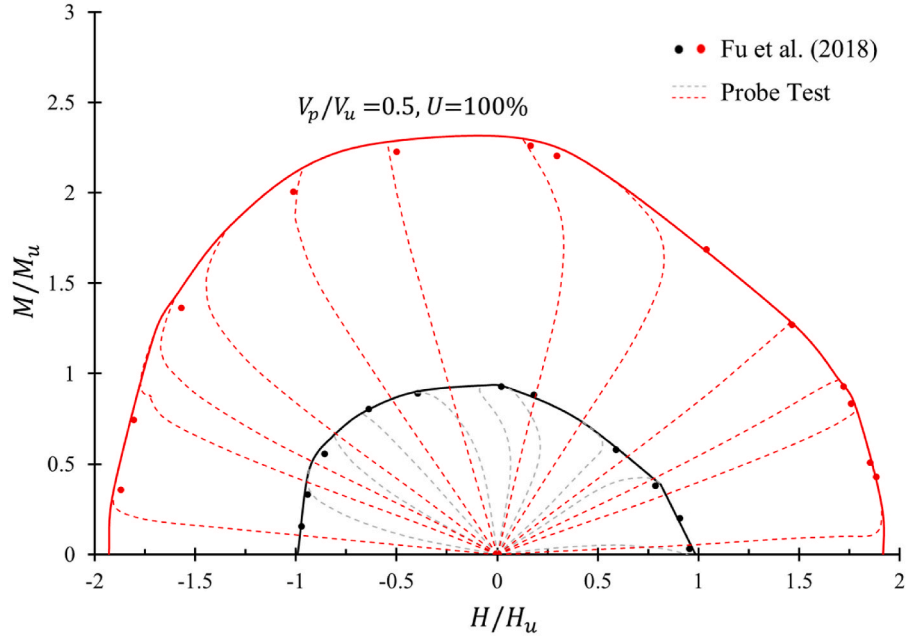

(b)

Fig. 3. Comparisons of the failure envelopes under: (a) V-H loading; (b) H-M loading.

3.2. Combined capacity

Fig. 3 presents the VH and HM failure envelopes of a skirted circular foundation with an aspect ratio $L/D = 0.2$, subjected to a preload $V_p = 0.5V_u$ and allowed to fully consolidate. The solid black line represents the failure envelope of the foundation without preloading, while the solid red line corresponds to the failure envelope after preloading and consolidation. It is evident that the finite element results from this study, both for the unconsolidated and preloaded with consolidated cases, show excellent agreement with the existing results reported by Fu et al. (2018). Additionally, the VH failure envelope obtained using the probe test is superimposed in Fig. 3a. The close alignment between this envelope and the one derived from the sideswipe method further validates the finite element model employed in this study.

4. Consolidated undrained uniaxial capacities

4.1. Undrained uniaxial capacities following full primary consolidation

The load-settlement responses of the caisson foundation under unconsolidated undrained conditions and after preloading with V_p/V_u ranging from 0.3 to 0.7, followed by full consolidation, are illustrated in

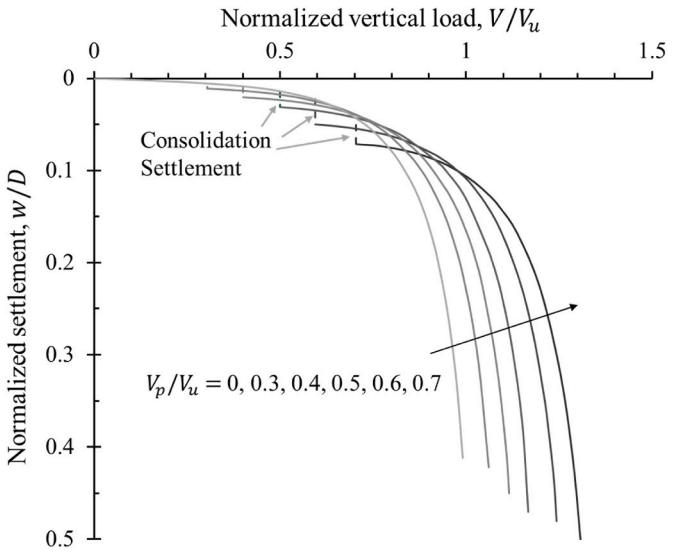

Fig. 4. Load-settlement response following preloading and full primary consolidation.

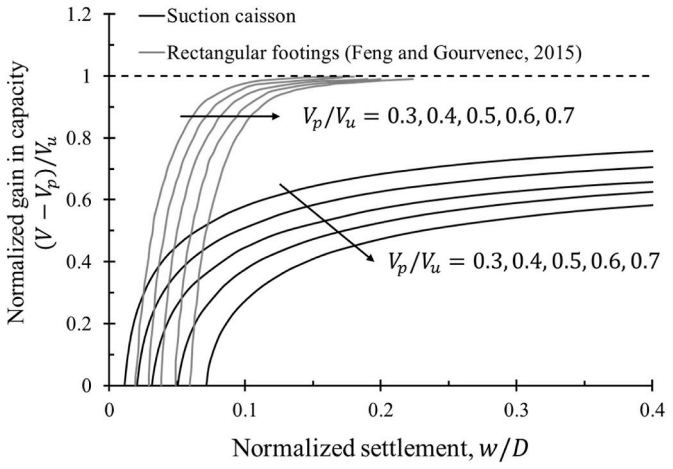

Fig. 5. Normalized gain in capacity after full consolidation.

Fig. 4. In the unconsolidated undrained case, the normalized vertical load V/V_u reaches a plateau at 1.0 without further increase. When the suction caisson is subjected to preloading and maintained for a certain period, settlement occurs due to consolidation. After consolidation is complete, the bearing capacity during re-penetration typically increases by a fraction proportional to the preload level. For surface rectangular footings or skirted foundations with low aspect ratios, the increase in vertical bearing capacity ($V/V_u - 1$) is generally consistent with the magnitude of the preload V_p (Feng and Gourvenec, 2015; Fu et al., 2018). This is because the soil region that experiences strength gain from the dissipation of preload-induced excess pore pressure substantially overlaps with the failure mechanism mobilized during subsequent vertical loading, allowing for a nearly full realization of the potential capacity increase. However, for skirted foundations with higher aspect ratios, such as the suction caisson with L/D = 1.5 examined in this study, the gain in capacity does not fully reach the applied preload V_p (Fig. 5). This can be attributed to the longer skirt, which, although having limited influence on the vertical extent of excess pore pressure which typically distributed up to 0.5D below the skirt tip (Gourvenec and Randolph, 2010; Zhang et al., 2024), significantly restricts the lateral dissipation of excess pore pressure beneath the foundation. Moreover, the extended skirt increases the share of penetration resistance contributed by skirt friction, reduces the contact pressure at both the top lid and the skirt tip, thereby restricting the development of excess pore pressure within the skirt compartment. As a result, the overlapping area between the foundation failure mechanism and the zone of soil strength improvement is diminished, the enhancement in bearing capacity after consolidation is reduced.

Fig. 6 illustrates the enhancement in bearing capacity of the suction caisson under different loading directions after full consolidation at various preload degrees. The smallest gain was observed in the vertical direction as the failure mechanism of the vertically loaded foundation exhibits the least overlap with the zone of soil strength improvement compared with other loading directions, resulting in the smallest enhancement in vertical bearing capacity. For foundations subjected to vertical preloading and subsequent consolidation, Gourvenec et al. (2014) proposed a method to predict the increase in bearing capacity based on the gain in operative undrained strength. After preloading and consolidation, the improvement in shear strength of the soil beneath the foundation can be expressed as:

$$\Delta s_u = f_{s_u} f_\sigma R \frac{V_p}{A} \tag{4}$$

where f_{s_u} is a shear strength factor to account for the non-uniform distribution of the increase in shear strength, f_σ is a stress factor to account for the non-uniform distribution of stress in the soil zone affected by preload, R is the normally consolidated undrained strength ratio s_u/σ'_v accounting for different soil properties(Eq. (3)). In normally consolidated soils, the scaling factor $f_{s_u} f_\sigma$ is independent of both foundation geometry and soil properties so it can be treated as a single unified parameter for simplicity. The enhancement in bearing capacity after full consolidation can be derived directly from the increase in shear strength, as expressed by the following relationship:

$$\frac{V_f}{V_u}, \frac{H_f}{H_u}, \frac{M_f}{M_u}, \frac{T_f}{T_u} = 1 + \frac{\Delta s_u}{s_u} = 1 + f_{s_u} f_\sigma R N_{cv} \frac{V_p}{V_u} \tag{5}$$

By applying this approach, the enhancement in bearing capacity under various preload degrees and loading directions was fitted, as shown in Fig. 6. It is evident that Eq. (5) fails to accurately capture the variation of capacity increase with preload degree. The results exhibit a quadratic growth trend, with a significantly lower rate of increase at low preload degree ($V_p/V_u = 0.1$) compared to higher preload degrees. This behavior can be attributed to the fact that the volumetric change induced by elastic compression under low preload degrees is substantially smaller than that caused by plastic compression at higher preload levels. As a result, the improvement in soil strength beneath the foundation remains limited under small preload magnitudes (Fu et al., 2015). This quadratic growth trend is typically observed in foundations with aspect ratios L/D greater than 0.5(Vulpe et al., 2016; Fu et al., 2017). The extended skirt further diminishes the modest strength improvement resulting from low preload degrees. If it is assumed that the enhancement in soil strength or post-consolidation bearing capacity initiates from a preload level βV_u that is lower than the unconsolidated undrained capacity, or if the case of $V_p/V_u = 0.1$ which is less useful in practical engineering is excluded, Eq. (5) can be reformulated as follows (Gourvenec et al., 2014; Zhang et al., 2024):

$$v_f, h_f, m_f, t_f = \frac{V_f}{V_u}, \frac{H_f}{H_u}, \frac{M_f}{M_u}, \frac{T_f}{T_u} = 1 + f_{s_u} f_\sigma R N_{cv} \left(\frac{V_p}{V_u} - \beta \right) \tag{6}$$

For notational convenience, the normalized capacities after full consolidation relative to the unconsolidated undrained bearing capacity are denoted as v_f, h_f, m_f, t_f for vertical, horizontal, moment, and torsional loading, respectively. Based on the finite element results, the values of the scaling factor $f_{s_u} f_\sigma$ and the parameter β in Eq. (6) were determined and are summarized in Table 2. As illustrated in Fig. 6, the proposed expression provides a more accurate prediction of the enhancement in uniaxial bearing capacity after consolidation for suction caissons with an

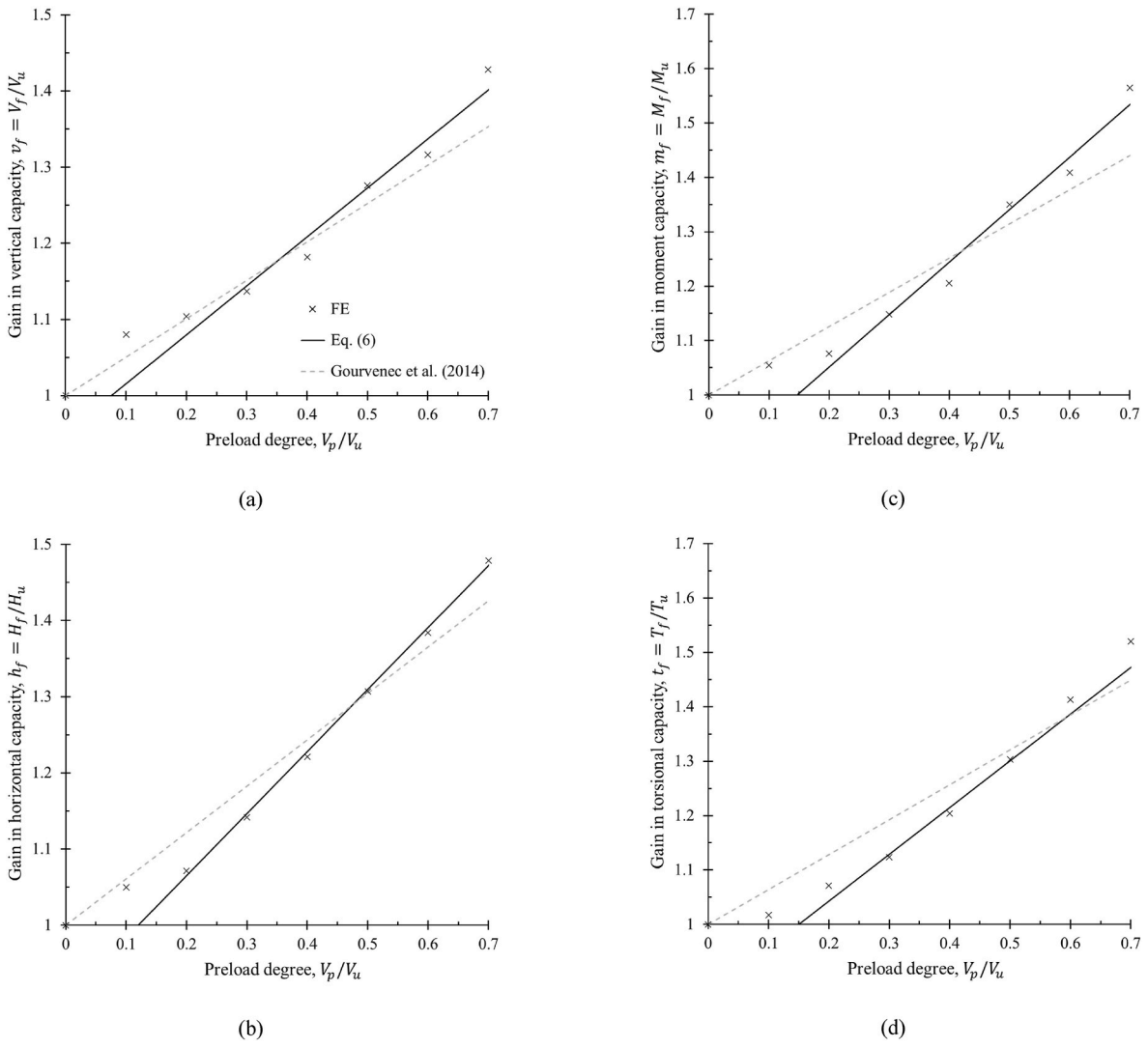

Fig. 6. Uniaxial capacities gain due to preloading and full primary consolidation in: (a) vertical; (b) horizontal; (c) moment; (d) torsional directions.

Table 2
Parameters for predicting the consolidated capacity gain.

	V_f/V_u	H_f/H_u	M_f/M_u	T_f/T_u
$f_{s_u}f_\sigma$	0.64	0.81	0.96	0.86
β	0.076	0.120	0.146	0.151

aspect ratio $L/D = 1.5$.

4.2. Undrained uniaxial capacities following partial consolidation

In practice, due to constraints in the construction schedule, foundations often enter service before full consolidation is achieved. Therefore, the ability to accurately predict the bearing capacity under partial consolidation is of significant practical importance. Establishing the time-settlement response of the suction caisson as a function of the preload degree is an essential prerequisite. Fig. 7 illustrates the time-settlement behavior of the caisson foundation under different preload levels. The dimensionless time factor T_s can be expressed as:

$$T_s = \frac{c_{v0}t_c}{D^2} \tag{7}$$

The consolidation settlement of the foundation, when normalized by

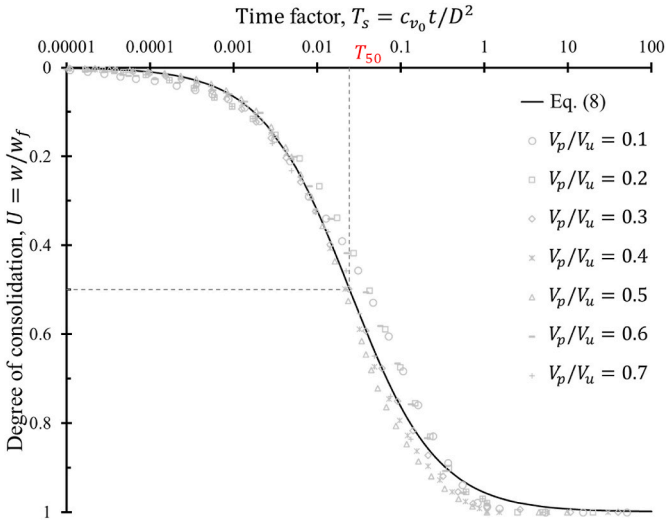

Fig. 7. Time-settlement response of the suction caisson under different preload degree.

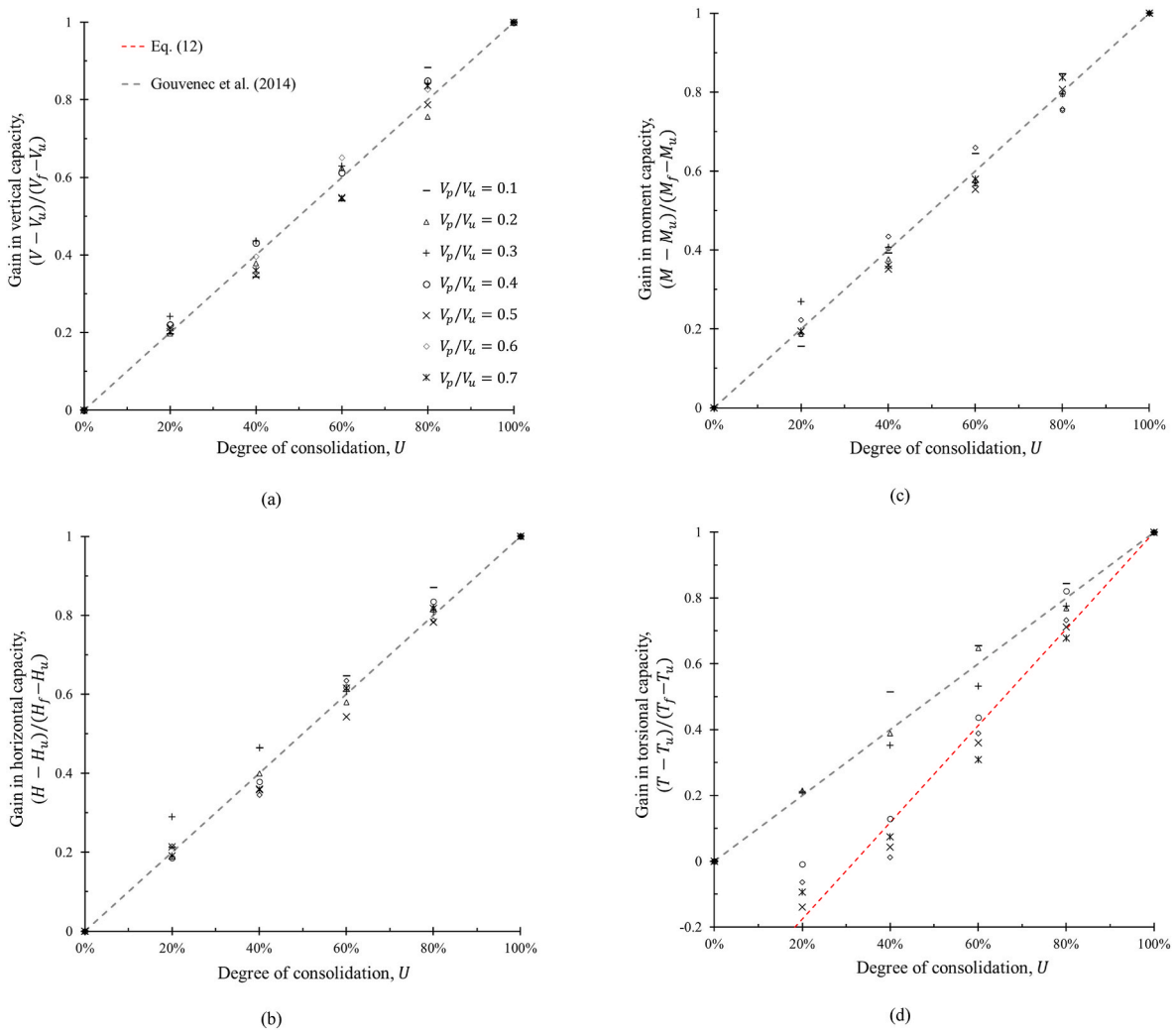

Fig. 8. Capacity gain against degree of consolidation in: (a) vertical; (b) horizontal; (c) moment; (d) torsional directions.

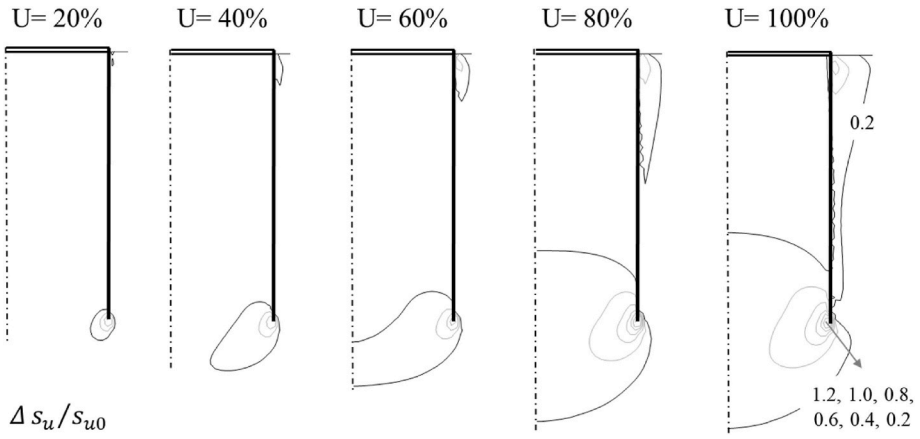

Fig. 9. Contours of shear strength gain $(V_p/V_u = 0.5)$ at intervals of $0.2\Delta s_u/s_{u0}$

the final consolidation settlement, can be represented as a hyperbolic function of the dimensionless time factor T_s, which can effectively capture the consolidation response under different preload degrees, as expressed by:

$$U = \frac{w}{w_f} = \frac{1}{\left(1 + \frac{T_s}{T_{50}}\right)^{\Lambda}} \tag{8}$$

where T_{50} denotes the value of the dimensionless time factor when the consolidation settlement reaches half of the final value, taken as 0.023 in

this study, and Λ is a fitted constant with a value of −0.82.

Following an extension of the work-hardening rule proposed by Bransby (2002), which links consolidation settlement to bearing capacity, Gourvenec et al. (2014) introduced a relationship between normalized bearing capacity enhancement and the degree of consolidation to predict the magnitude of capacity improvement. Fig. 8 illustrates the relationship between the increase in bearing capacity and the degree of consolidation under different preload levels. It can be observed that the enhancement in bearing capacity generally exhibits a nearly 1:1 linear relationship with the degree of consolidation. However, under higher preload degrees ($V_p/V_u > 0.4$), the torsional capacity initially decreases and then increases with the degree of consolidation, following a quadratic trend, which can be attributed to the extent and distribution of shear strength improvement in the soil beneath the foundation.

Fig. 9 presents contours of the normalized increase in shear strength, $\Delta s_u/s_{u0}$, under a preload of $V_p = 0.5V_u$ at various consolidation degrees. The enhancement in soil shear strength results from the dissipation of pore water and the consequent reduction in void ratio. In the MCC model, the increase in shear strength $\Delta s_u/s_{u0}$ can be expressed as follows (Stanier and White, 2019):

$$\frac{\Delta s_u}{s_{u0}} = \frac{s_{uf}}{s_{u0}} - 1 = \exp\left(\frac{e_0 - e}{\lambda}\right) - 1 \tag{9}$$

where Δs_u represents the difference between the post-consolidation shear strength s_{uf} and the initial shear strength s_{u0}, e_0 denotes the initial void ratio, e is the void ratio after consolidation, and λ is the virgin compression index. Additionally, the general expression for the ultimate torsional capacity of the caisson foundation in normally consolidated soil is given as follows for better explanation:

$$T_{NC} = \frac{\pi\rho L^2 D^2}{4} + \frac{\pi\rho L D^3}{12} \tag{10}$$

where ρ is the undrained shear strength gradient with depth. As indicated in Eq. (10), the bearing capacity of the caisson foundation is primarily contributed by the shear strength of the soil along the external skirt wall and beneath the foundation lid. During the early stages of consolidation, the zone of shear strength improvement is mainly concentrated near the skirt tip, contributing little to the enhancement of torsional capacity (Fig. 9). Moreover, higher preload degree can lead to a reduction in the foundation's torsional resistance. Consequently, under significant preload conditions, the torsional capacity of the caisson may initially decrease compared to that of the no-preload foundation. As the degree of consolidation increases, the shear strength of the soil inside the caisson and along the external skirt gradually improves, leading to a subsequent enhancement of the torsional capacity. For the cases with preload degrees between 0.4 and 0.7, the relationship between the increase in torsional capacity and the degree of consolidation can be fitted by the following expression:

$$\frac{T - T_u}{T_f - T_u} = 1.47U - 0.47 \tag{11}$$

Based on the relationship between bearing capacity enhancement and the degree of consolidation shown in Fig. 8, the dimensionless increase in bearing capacity normalized by the unconsolidated undrained bearing capacity after partial consolidation can be derived as follows:

$$v_p = \frac{V}{V_u} = 1 + U\left(\frac{V_f}{V_u} - 1\right) = 1 + U(v_f - 1) \tag{12a}$$

$$h_p = \frac{H}{H_u} = 1 + U\left(\frac{H_f}{H_u} - 1\right) = 1 + U(h_f - 1) \tag{12b}$$

$$m_p = \frac{M}{M_u} = 1 + U\left(\frac{M_f}{M_u} - 1\right) = 1 + U(m_f - 1) \tag{12c}$$

For $0 < V_p/V_u < 04$:

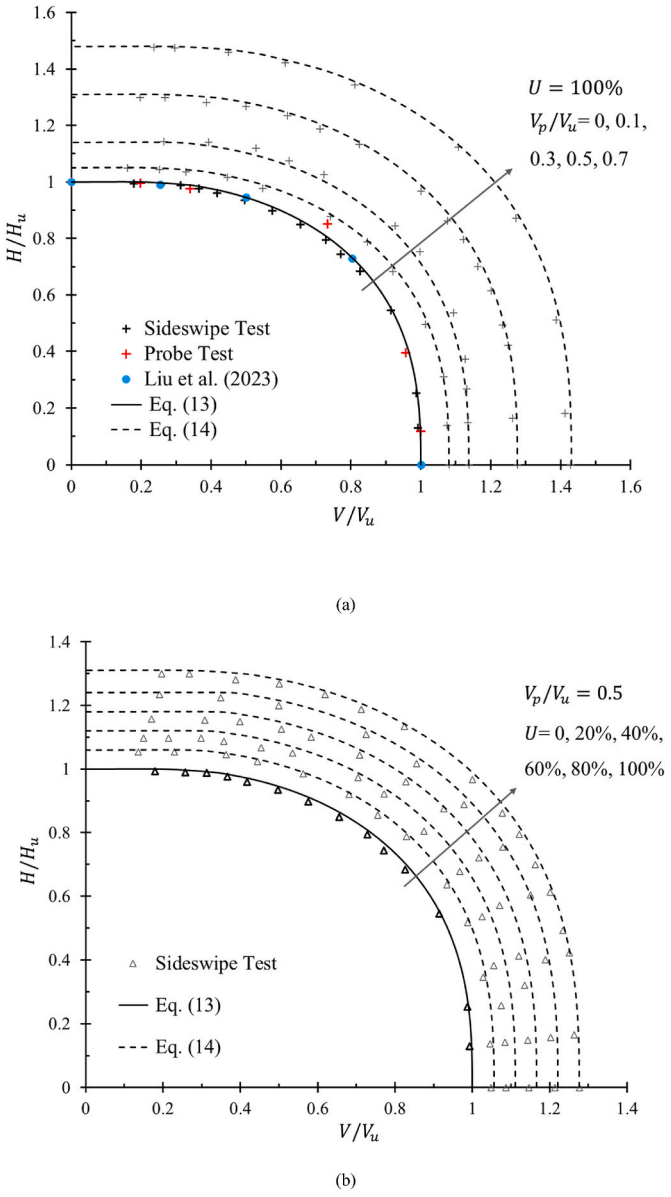

Fig. 10. Failure envelope for combined V-H loading with: (a) varying preload degree (b) different duration of preloading.

$$t_p = \frac{T}{T_u} = 1 + U\left(\frac{T_f}{T_u} - 1\right) = 1 + U(t_f - 1) \tag{12d}$$

For $0.4 \le V_p/V_u \le 0.7$:

$$t_p = \frac{T}{T_u} = 1 + (1.47U - 0.47)\left(\frac{T_f}{T_u} - 1\right) = 1 + (1.47U - 0.47)(t_f - 1) \tag{12e}$$

5. Consolidated undrained capacity under V-H-M-T loading

5.1. V-H loading plane

Fig. 10a presents the dimensionless VH failure envelopes of the caisson foundation after full consolidation under different preload degree, where both vertical and horizontal loads are normalized by the unconsolidated undrained bearing capacity. This study considers four distinct preload degrees ($V_p/V_u = 0.1, 0.3, 0.5, 0.7$) and five degrees of consolidation $U = 0.2, 0.4, 0.6, 0.8, 1.0$. The failure envelopes were fitted

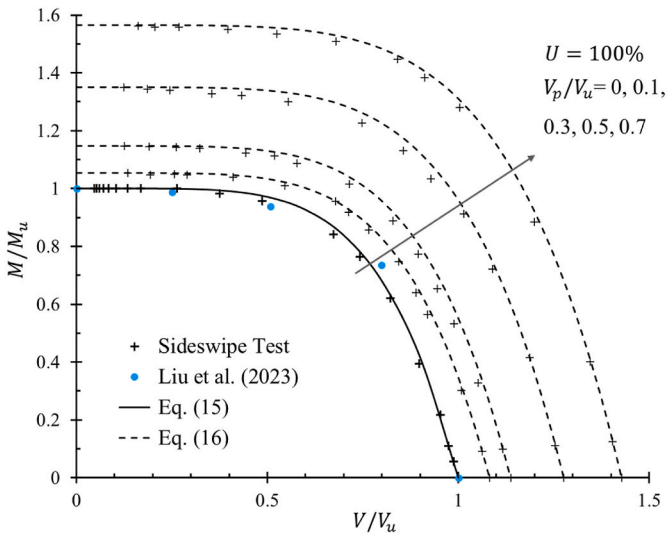

(a)

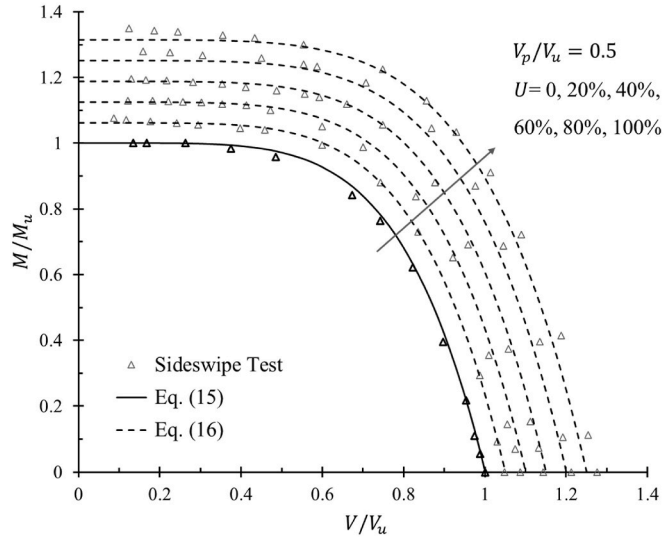

(b)

Fig. 11. Failure envelope for combined V-M loading with: (a) varying preload degree (b) different duration of preloading.

based on results obtained from swipe tests or probe tests. For further validation, existing failure envelopes for suction caissons with an aspect ratio of 1.5 are also plotted in Fig. 10a to ensure the accuracy of the reference envelope representing the unpreloaded and unconsolidated condition.

The innermost envelope corresponds to the failure envelope of the caisson without preloading, which can be described using a piecewise function (Gourvenec, 2008):

For $V/V_u < 0.2$:

$$\frac{H}{H_u} = 1 \tag{13a}$$

For $0.2 \le V/V_u < 1.0$:

$$\frac{V}{V_u} = 0.2 + 0.8\left[1 - \left(\frac{H}{H_u}\right)^{2.7}\right]^{0.5} \tag{13b}$$

Compared to the unconsolidated condition, the failure envelopes after preloading and full consolidation expand to varying degrees, reflecting the enhancement in bearing capacity due to consolidation. However, this expansion is not proportional, as the increases in undrained uniaxial capacities are not uniform across different loading directions. This is evident in the intercepts of the envelope along the coordinate axes, which represent the improvements in vertical and horizontal bearing capacities under the given preload level. Therefore, the failure envelope after full consolidation under any preload degree can be obtained by replacing V_u and H_u in Eq. (13) with vV_u and hH_u, respectively:

For $V/V_u < 0.2v$:

$$\frac{H}{H_u} = h \tag{14a}$$

For $0.2v \le V/V_u < 1.0v$:

$$\frac{V}{V_u} = v\left\{0.2 + 0.8\left[1 - \left(\frac{H}{hH_u}\right)^{2.7}\right]^{0.5}\right\} \tag{14b}$$

Note that when determining the failure envelope after full consolidation, the parameters v and h in Eq. (14) and the subsequent expressions for failure envelope in other loading planes should be taken as the gains in uniaxial capacities after full consolidation, denoted v_f and h_f (Eq. (6)). Similarly, for the failure envelope under partial consolidation, the corresponding gains v_p and h_p (Eq. (12)) should be used.

The failure envelopes of the caisson foundation under partial consolidation are plotted in Fig. 10b. As with the fully consolidated case, the expansion of these envelopes is non-uniform, reflecting the differing degrees of enhancement in uniaxial capacities along various loading directions during partial consolidation. The proposed expression in Eq. (14) effectively captures the shape of the partially consolidated failure envelopes when the gains v_p and h_p are incorporated.

5.2. V-M loading plane

The normalized VM failure envelopes are depicted in Fig. 11. Similar to previous observations, the expansion of these envelopes is non-uniform; however, the shapes of the expanded envelopes remain geometrically similar to that of the no-preload and unconsolidated case. This indicates that the consolidated failure envelopes can be expressed as a function of the unconsolidated undrained failure envelope scaled by the gains in consolidated undrained uniaxial capacities. The unconsolidated envelope remains the smallest. The intercepts of the expanded envelopes on the coordinate axes are determined by the increases in undrained uniaxial capacities after consolidation. The unconsolidated failure envelope can be fitted using a simple power function: (Gourvenec and Randolph, 2003):

$$\frac{V}{V_u} = \left(1 - \frac{M}{M_u}\right)^{a} \tag{15}$$

For the unconsolidated VM failure envelope, the value of a is primarily influenced by the aspect ratio L/D of the suction caisson and shows little correlation with soil strength heterogeneity, a higher aspect ratio corresponds to a smaller value of a. Fu et al. (2018) investigated the failure envelopes of suction caissons with an aspect ratio of 0.2 under varying soil strength heterogeneity and found that $a = 0.24$ provides the best fit. For caissons with aspect ratios between 0 and 1.0, Chen et al. (2023) observed that a constant value of $a = 0.25$ accurately describes the lower bound of the VM failure envelope. For caissons with aspect ratios ranging from 1.0 to 2.0, the size of the failure envelope remains similar, and a constant value of $a = 0.18$ can effectively represent the VM failure envelope (Liu et al., 2023). In this study, $a = 0.20$ was found to best fit the VM failure envelope of the suction caisson with an aspect ratio of 1.5. The expanded failure envelope after consolidation can be expressed as:

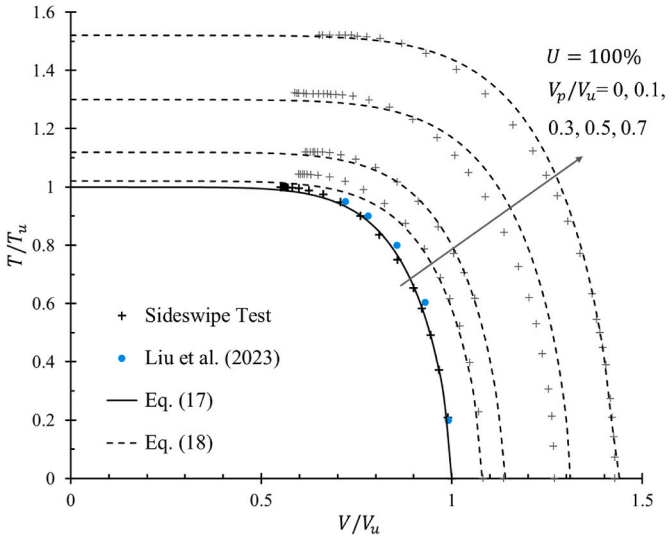

Fig. 12. Failure envelope for combined V-T loading with varying preload degree.

$$\frac{V}{vV_u} = \left(1 - \frac{M}{mM_u}\right)^{0.2} \tag{16}$$

As shown in Fig. 11, Eq. (16) provides a good fit to the consolidated VM failure envelopes.

5.3. V-T loading plane

The failure envelopes under combined VT loading are presented in Fig. 12. The expansion of these envelopes is highly non-uniform, primarily due to the limited gain in torsional capacity after consolidation at lower preload degrees. The unconsolidated failure envelope can be expressed as:

$$\left(\frac{V}{V_u}\right)^7 + \left(\frac{T}{T_u}\right)^{1.56} = 1 \tag{17}$$

Similar to VH and VM failure envelope, the consolidated failure envelope in VT loading plane can be expressed as:

$$\left(\frac{V}{vV_u}\right)^7 + \left(\frac{T}{tT_u}\right)^{1.56} = 1 \tag{18}$$

Fig. 13 illustrates the influence of different preload degrees and consolidation durations on the VT failure envelopes. Fig. 13a shows the envelopes at a preload degree of 0.1 under varying degrees of consolidation. It can be observed that the torsional capacity remains almost unchanged after consolidation. Furthermore, the finite element results for different preload degrees nearly all fall on the fitted curve of the VT envelope at $U = 1$, indicating that at very low preload levels, the bearing

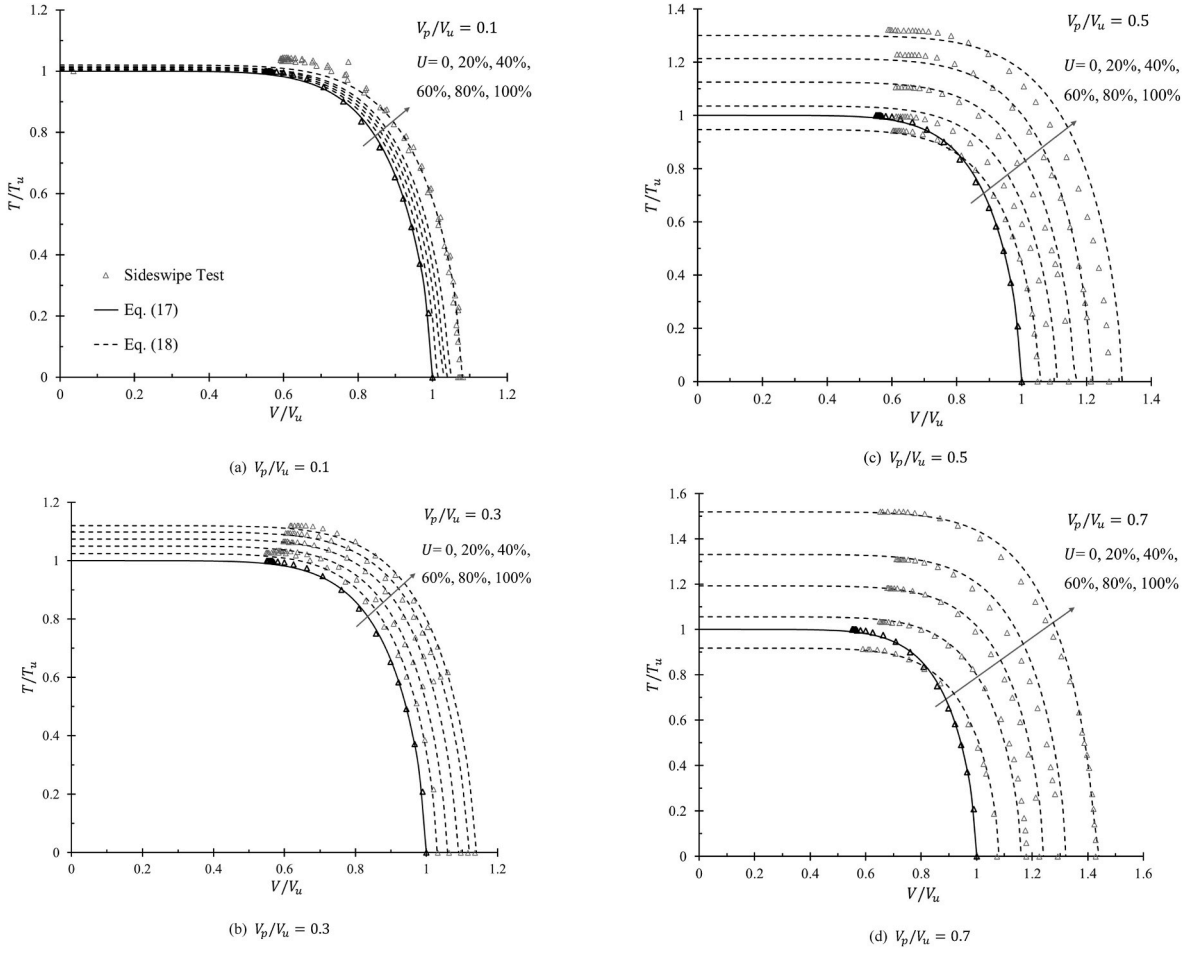

Fig. 13. Effects of duration of preloading on V-T failure envelope under different preload degree.

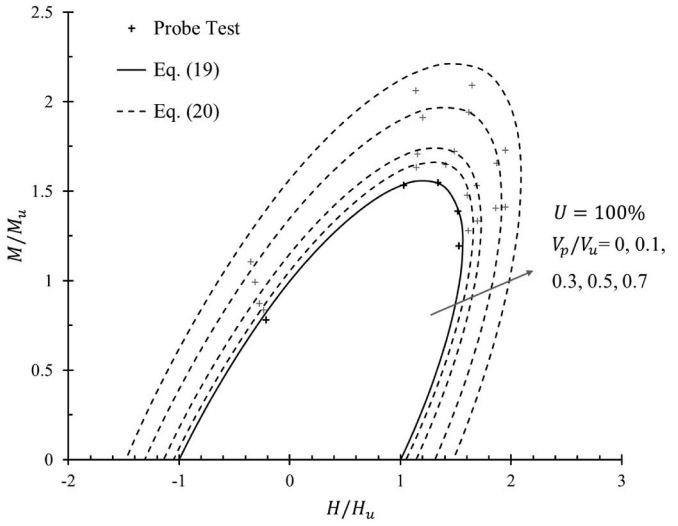

Fig. 14. Failure envelope for combined H-M loading with varying preload degree.

capacity increases rapidly with consolidation time. This behavior is reasonable, as the low preload generates limited excess pore pressure distributed over a small area, which dissipates quickly. However, this rapid stabilization does not occur at higher preload levels (Fig. 13a and b).

When the preload is higher and the consolidation time is short, the VT failure envelope may contract. This phenomenon is related to the reduction in torsional capacity under high preload degrees at low degrees of consolidation, as discussed earlier. The unconsolidated failure envelope reveals that torsional capacity begins to decrease when the vertical load exceeds 0.4 V_u. If the increase in capacity due to soil strength improvement is insufficient to offset this reduction, contraction of the envelope occurs (Fig. 13c and d).

Eq. (18) effectively captures both the expansion and contraction of the failure envelope under various conditions. It should be noted that at low preload degrees, although the envelope expands rapidly, the magnitude of expansion is limited. In such cases, the unconsolidated failure envelope may be conservatively adopted for design purposes.

5.4. Combined V-H-M failure envelope

The normalized H-M failure envelope after full consolidation under different preloading ratios are presented in Fig. 14,the unconsolidated failure envelope can be described by (Taiebat and Carter, 2005; Vulpe et al., 2014):

$$\left|\frac{H}{H_u}\right|^{1.95}+\left|\frac{M}{M_u}\right|^{1.95}-\delta\frac{HM}{H_uM_u}=1 \tag{19}$$

where δ is a fitting parameter related to the preload degree, taken in this study as $\delta = 1.53 - 0.2(V_p/V_u)$. The expanded failure envelope after consolidation can be represented as:

$$\left|\frac{H}{hH_u}\right|^{1.95}+\left|\frac{M}{mM_u}\right|^{1.95}-\delta\frac{HM}{hH_umM_u}=1 \tag{20}$$

It can be observed that Eq. (20) slightly overestimates the bearing capacity of the caisson at a preload degree of 0.7. However, such high preload levels are uncommon in practical engineering, so this overestimation does not significantly affect the applicability of the results.

Fig. 15 illustrates the influence of consolidation time on the H-M failure envelopes at preload degrees of 0.3 and 0.5. Clearly, the expansion of the failure envelopes with consolidation time is proportional, and higher preload degrees lead to greater expansion. At a preload degree of

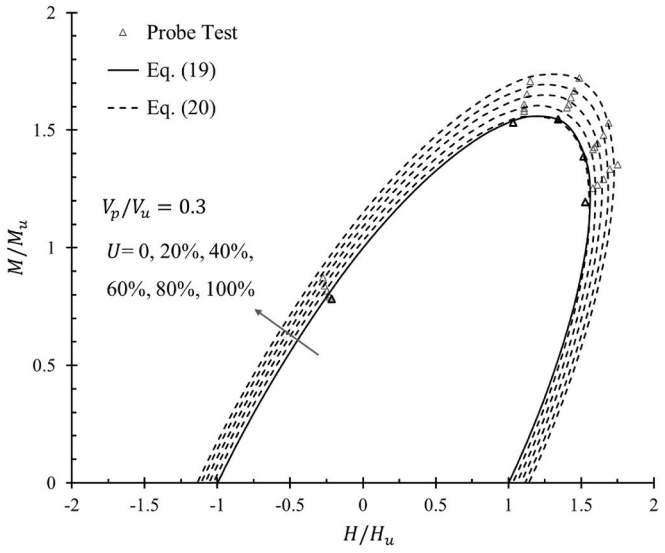

(a) $V_p/V_u = 0.3$

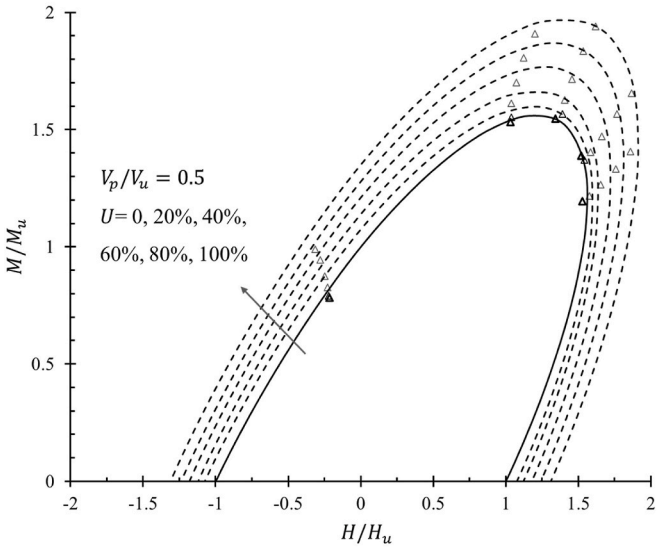

(b) $V_p/V_u = 0.5$

Fig. 15. Effects of duration of preloading on H-M failure envelope under different preload degree.

0.3, the expansion of the envelope remains limited, and a slight contraction occurs during the early stages of consolidation. This behavior is similar to the contraction observed in the V-T failure envelopes. When the caisson subjected to a vertical load that is a certain proportion of its ultimate vertical bearing capacity, the HM failure envelope will contract to a corresponding extent based on the magnitude of the vertical load (Gourvenec and Barnett, 2011; Vulpe, 2015). In the early consolidation stage, the improvement in bearing capacity due to soil strength gain is insufficient to counteract the contraction induced by the vertical load, resulting in a temporary shrinkage of the H-M envelope. In contrast, at a preload degree of 0.5, the substantial soil strength improvement outweighs the contraction effect, preventing any reduction in the envelope size.

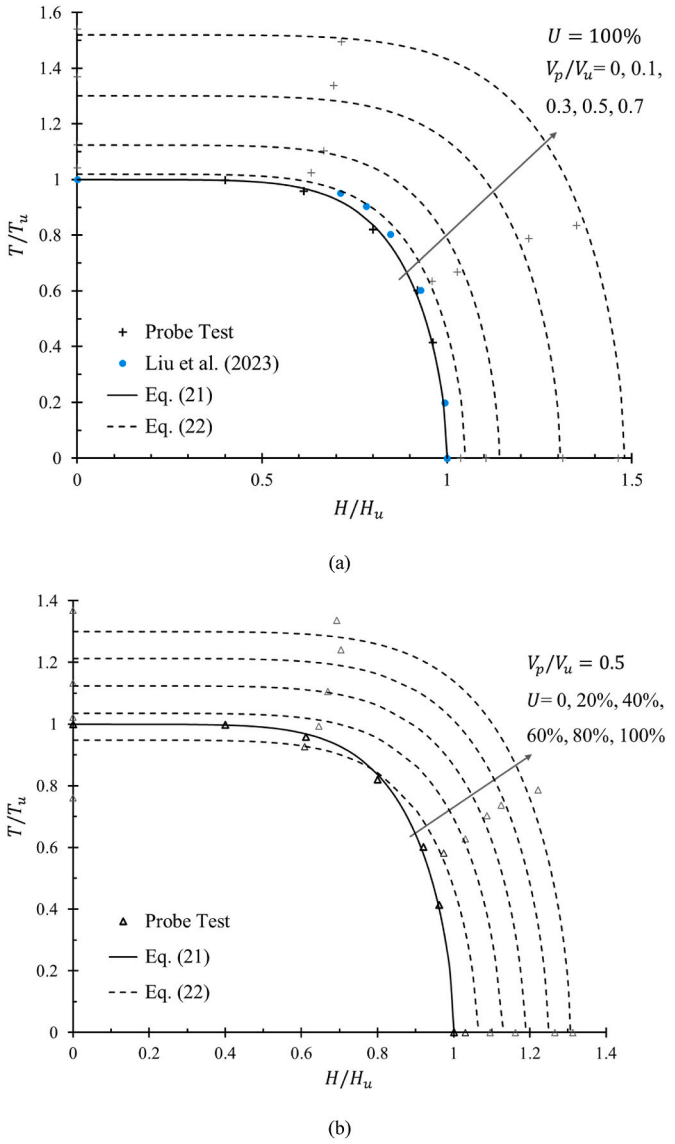

Fig. 16. Failure envelope for combined H-T loading with: (a) varying preload degree (b) different duration of preloading.

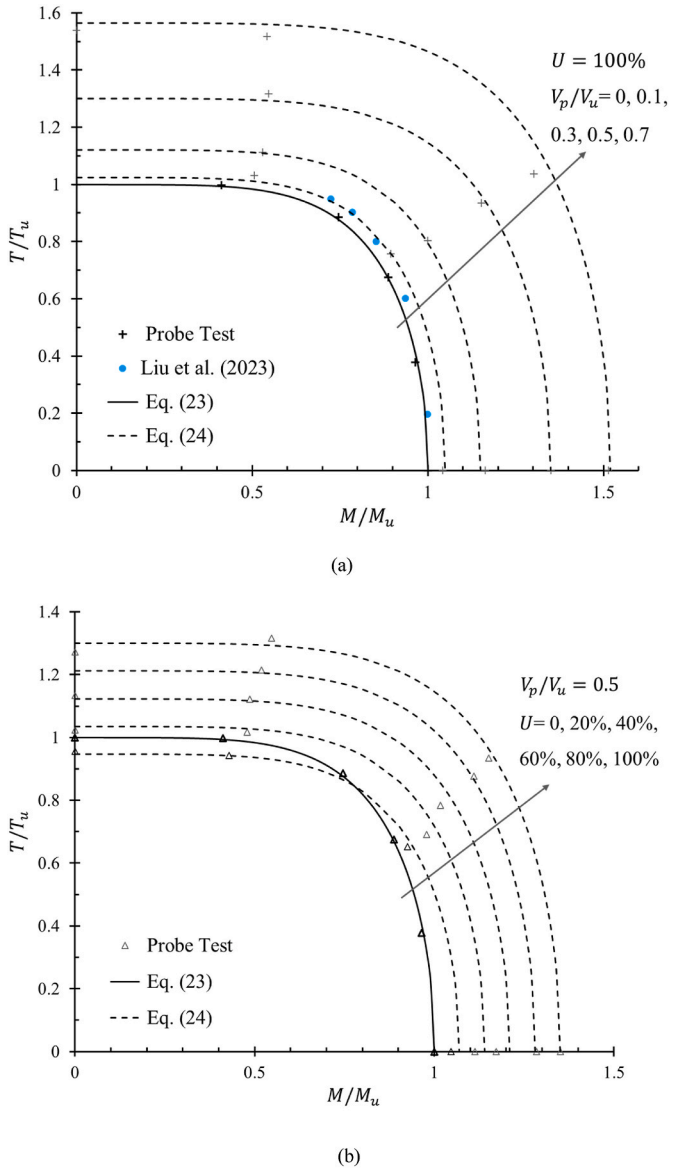

Fig. 17. Failure envelope for combined M-T loading with: (a) varying preload degree (b) different duration of preloading.

5.5. Combined T-H-M failure envelope

Similar to the influence of vertical load, torsional loading also affects the size and shape of the H-M failure envelope. For surface rectangular foundations, the magnitude of torsion significantly alters both the shape and size of the H-M envelope (FENG et al., 2014). In contrast, for surface circular foundations (Shen et al., 2017) and caisson foundations (Li et al., 2019; Chen et al., 2023), torsion does not change the shape of the envelope but influences its size by modifying the uniaxial capacities. Therefore, the complete T-H-M failure envelope can be derived by replacing H/H_u and M/M_u in the normalized H-M envelope with functions accounting for the effect of torsion.

The H-T failure envelopes under different preload degrees and degrees of consolidation are presented in Fig. 16 and can be represented as follows (Finnie and Morgan, 2004):

$$\left(\frac{H}{H_u}\right)^6 + \left(\frac{T}{T_u}\right)^{1.7} = 1 \tag{21}$$

$$\left(\frac{H}{hH_u}\right)^6 + \left(\frac{T}{tT_u}\right)^{1.7} = 1 \tag{22}$$

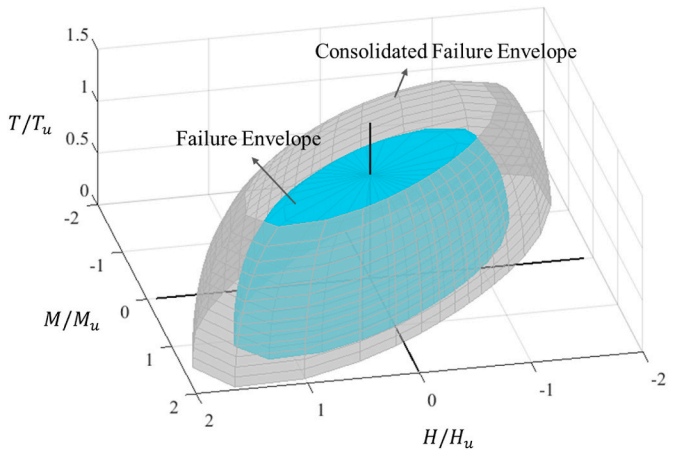

Fig. 18. Consolidated failure envelope ($V_p/V_u = 0.5, U = 100\%$) compared with original failure envelope in THM space.

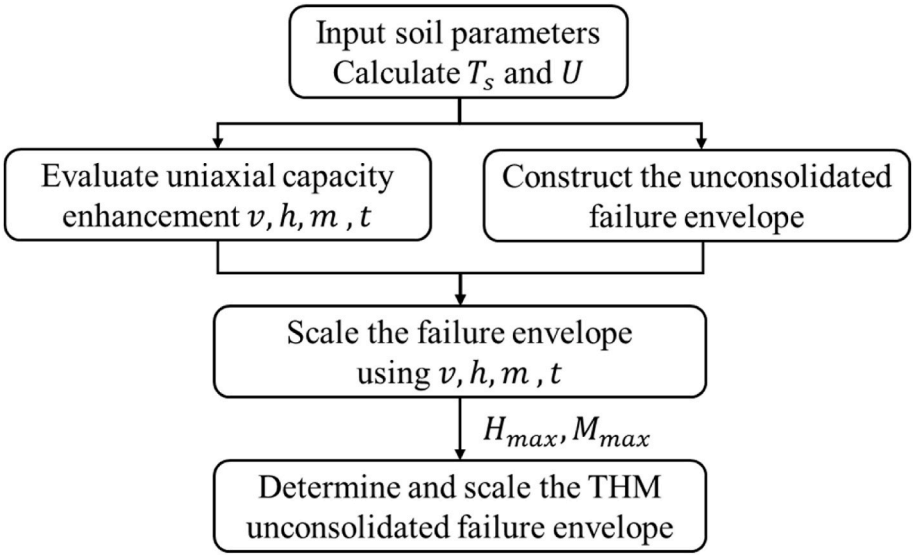

Fig. 19. Design procedure for predicting consolidated failure envelope.

At a low preload degree ($(V_p/V_u = 0.1)$, the fully consolidated envelope shows limited expansion due to the small improvement in uniaxial capacities after consolidation (Fig. 16a). Under a preload degree of 0.5, contraction of the consolidated envelope occurs again at short consolidation times, which remains attributable to the evolution of torsional uniaxial capacity with consolidation duration (Fig. 16b).

Fig. 17 illustrates the failure envelopes of the caisson under combined M-T loading. The unconsolidated and consolidated failure envelopes can be represented by the following expressions:

$$\left(\frac{M}{M_u}\right)^5 + \left(\frac{T}{T_u}\right)^2 = 1 \tag{23}$$

$$\left(\frac{M}{mM_u}\right)^5 + \left(\frac{T}{tT_u}\right)^2 = 1 \tag{24}$$

Thus, the T-H-M failure envelope of the suction caisson can be expressed as:

$$\left|\frac{H}{H_{\max}}\right|^{1.95} + \left|\frac{M}{M_{\max}}\right|^{1.95} - \left(1.53 - 0.2\frac{V_p}{V_u}\right)\frac{HM}{H_{\max}M_{\max}} = 1 \tag{25}$$

where $H_{\max}$ and $M_{\max}$ represent the reduced or enhanced horizontal and moment capacities, respectively, after the foundation is subjected to torsion or undergoes preloading and consolidation followed by torsional loading. Their values can be determined using Eq. (22) (24). Fig. 18 illustrates the expansion of the failure envelope in the T-H-M space for a suction caisson under a preload degree of 0.5 after full consolidation. Since torsion has minimal influence on the shape of the H-M envelope and primarily affects the uniaxial capacities, the H-M envelope is assumed to remain geometrically similar but scales in size with increasing torsion. The H-M envelope gradually contracts as the torsional load increases, until a critical torsional value is reached, beyond which it shrinks abruptly, resulting in a T-H-M failure envelope resembling an elliptical plateau in shape.

6. Design procedure

The undrained combined bearing capacity of a caisson foundation under various preload levels and consolidation times can be predicted by the following procedure in the flowchart (Fig. 19).

Note that although the current study focuses on a single suction caisson with L/D = 1.5, existing research suggests that the bearing capacity envelopes for caissons with aspect ratios between 1 and 2 can be

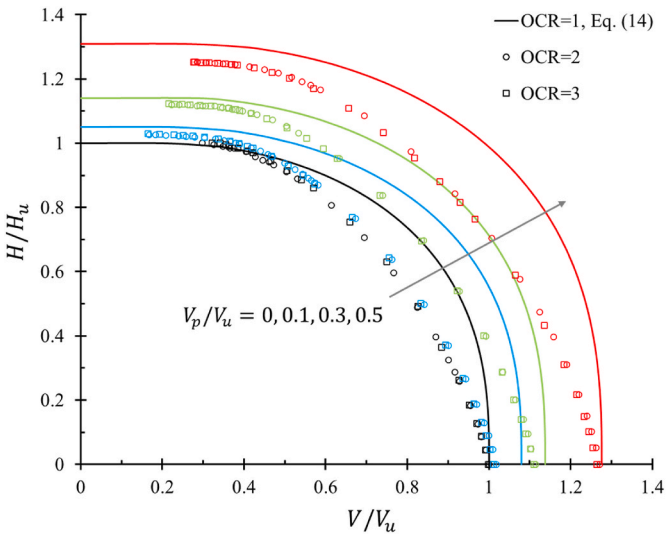

Fig. 20. Failure envelope for combined V-H loading with different OCR.

reasonably approximated using expressions derived for L/D = 1.5 (Liu et al., 2023). However, the H-M failure envelope must be independently evaluated for different aspect ratios, as the failure mechanism is highly sensitive to skirt length. Therefore, while the proposed design framework can theoretically be extended to suction caissons with aspect ratios ranging from 1 to 2, the H-M failure envelope should be reassessed specifically for each geometry. All other unconsolidated or consolidated failure envelopes can be directly applied based on the results presented in this study.

The study in this paper is primarily based on normally consolidated clay. However, in many regions worldwide, such as the North Sea and the Gulf of Mexico, marine soils are mainly composed of normally consolidated or lightly over-consolidated clay, with an over-consolidation ratio (OCR) typically ranging between 1 and 3. As shown in Fig. 20, for suction caissons with an aspect ratio of 1.5 under combined V-H loading in soils with different OCR, the failure envelope shrinks considerably. This reduction is mainly reflected in the change in shape and the diminished increase in consolidated uniaxial bearing capacity (Zdravkovic et al., 2003). Nevertheless, the shape of the failure envelope after consolidation remains consistent with that before

consolidation, indicating that the expansion of the failure envelope in over-consolidated soils after consolidation can still be predicted using the methodology outlined in Fig. 19.

7. Conclusions

This study conducted a series of three-dimensional coupled finite element analyses to investigate the changes in uniaxial bearing capacity and failure envelopes of suction caissons after consolidation under different preload degrees and degrees of consolidation. A simplified method for predicting the consolidated failure envelope of suction caissons is proposed. The main findings are summarized as follows.

The consolidated undrained uniaxial bearing capacity can be predicted using a theoretical critical state soil mechanics framework, based on a simple linear relationship with the preload degree and the degree of consolidation.

High vertical preload levels significantly reduce the torsional capacity of the foundation and may even lead to contraction of the failure envelope during the early stages of consolidation.

After preloading, the soil strength improvement zone initially concentrates near the skirt tip. As the degree of consolidation increases, this zone gradually expands to encompass the region beneath the foundation and along the external side of the skirt wall.

The normalized consolidated failure envelope can be derived by scaling the unconsolidated undrained normalized failure envelope according to the corresponding gains in uniaxial capacities after consolidation, expressed as a function of preload magnitude and duration.

CRediT authorship contribution statement

Hao Ran Li: Writing – review & editing, Writing – original draft, Validation, Software, Methodology, Investigation, Data curation, Conceptualization. **Xiu Zhe Wang:** Writing – review & editing, Software, Methodology, Investigation, Formal analysis, Conceptualization. **Jiang Tao Yi:** Writing – review & editing, Supervision, Resources, Methodology, Funding acquisition. **Hong Yu Tang:** Writing – review & editing, Software. **Xiao Han:** Writing – review & editing, Data curation.

Declaration of competing interest

The authors declare that they have no known competing financial interests or personal relationships that could have appeared to influence the work reported in this paper.

Acknowledgments

The authors wish to acknowledge the research funding provided by the National Natural Science Foundation of China (Grant number: 52371259, 52221002).

Nomenclature

A	Cross-sectional area of the foundation
c_{v0}	Initial coefficient of consolidation
D	Diameter of suction caisson
e	Void ratio after consolidation
e_0	Initial void ratio
e_N	e at $p' = 1$ kPa on the isotropic virgin consolidation line
f_{s_u}	Shear strength factor
f_σ	Stress factor
H	Horizontal load
$H_{\max}$	Horizontal capacities under torque
H_u	Ultimate undrained horizontal capacity
K_0	Coefficient of earth pressure at rest
k	Soil permeability
L	Skirt length
M	Moment load
M_{cs}	Slope of critical state line (CSL) in p' $-$ q space
$M_{\max}$	Moment capacities under torque
M_u	Ultimate undrained moment capacity
N_{cv}	Vertical bearing capacity factor
$p_0^{'}$	Mean effective stress
$p_{c0}^{'}$	Initial pre-consolidation pressure
R	Normally consolidated undrained strength ratio
s_u	Undrained shear strength
s_{u0}	Initial shear strength
s_{uf}	Post-consolidation shear strength
T	Torsional load
T_s	Dimensionless time factor
t_c	Consolidation time
t_w	Skirt thickness
U	Consolidation degree
V	Vertical load
V_p	Vertical preload
V_u	Ultimate undrained vertical capacity
V_f, H_f, M_f, T_f	Bearing capacity after full consolidation
v, h, m, t	Enhancement in bearing capacity

v_f, h_f, m_f, t_f Enhancement in bearing capacity after full consolidation
v_p, h_p, m_p, t_p Enhancement in bearing capacity after partial consolidation
γ_{sat} Saturated bulk unit weight
γ_w Unit weight of water
θ Lode angle
κ Swelling and recompression index
λ Virgin compression index
ν Poisson's ratio
ρ Undrained shear strength gradient
σ_v' Vertical effective stress
φ' Critical friction angle in triaxial compression
w Settlement
w_f Settlement after full primary consolidation

References

Alimoradi, H., Noorzad, A., Ebrahimian, B., 2024. Explicit FE analysis of 3D failure envelopes of suction caisson foundations supporting offshore wind turbines in sand subjected to combined loading. Ocean. Eng. 301, 116831.

Andersen, K.H., Murff, J.D., Randolph, M.F., Clukey, E.C., Erbrich, C.T., Jostad, H.P., Hansen, B., Aubeny, C., Sharma, P., Supachawarote, C., 2005. Suction anchors for deepwater applications. In: Proceedings of the International Symposium Frontiers in Offshore Geotechnics (ISFOG), Perth, pp. 3–32.

Bransby, F., 2002. The Undrained Inclined Load Capacity of Shallow Foundations After Con- Solidation Under Vertical Loads.

Bransby, M.F., Randolph, M.F., 1998. Combined loading of skirted foundations. Geotechnique 48 (5), 637–655.

Bransby, M.F., Yun, G.J., 2009. The undrained capacity of skirted strip foundations under combined loading. Geotechnique 59 (2), 115–125.

Bughi, S., Parker, E., 2011. Suction pile foundations: experience in the mediterranean offshore and installation feedback. In: ASME 2011, International Conference on Ocean. Offshore and Arctic Engineering, pp. 951–963.

Bye, A., Erbrich, C., Rognlien, B., Tjelta, T.I., 1995. Geotechnical design of bucket foundations. Proc. Annual Offshore Technology Conf. Houston. Paper OTC 7793.

Chen, H., Shen, Z., Wang, L., Tian, Y., Chu, X., 2023. Undrained capacity of skirted circular foundations under fully three-dimensional loading. Comput. Geotech. 156, 105261.

Dassault Systèmes, 2014. Abaqus Analysis User's Manual. Simulia, Providence, RI.

Fan, S., Zhang, Y., Li, S., Han, M., Liu, J., 2023. Correction and simplification of swipe category methods for determining the failure envelope on cohesive soil. Comput. Geotech. 164, 105853.

Feng, X., Gourvenec, S., 2015. Consolidated undrained load-carrying capacity of subsea mudmats under combined loading in six degrees of freedom. Geotechnique 65 (7), 563–575.

Feng, X., Randolph, M.F., Gourvenec, S., Wallerand, R., 2014. Design approach for rectangular mudmats under fully three-dimensional loading. Geotechnique 64 (1), 51–63.

Finnie, I.M.S., Morgan, N., 2004. Torsional loading of subsea structures. Proceedings of the 14th international offshore and polar engineering conference, Toulon, France.

Fu, D., Gaudin, C., Bienen, B., Tian, Y., Cassidy, M.J., 2018. Combined load capacity of a preloaded skirted circular foundation in clay. J. Geotech. Geoenviron. Eng. 144 (11), 4018084.

Fu, D., Gaudin, C., Tian, C., Bienen, B., Cassidy, M.J., 2015. Effects of preloading with consolidation on undrained bearing capacity of skirted circular footings. Geotechnique 65 (3), 231–246.

Fu, D., Gaudin, C., Tian, Y., Cassidy, M.J., Bienen, B., 2017. Uniaxial capacities of skirted circular foundations in clay. J. Geotech. Geoenviron. Eng. 143 (7), 4017022.

Fu, D., Zhou, Z., Yan, Y., Pradhan, D.L., Hennig, J., 2021. A method to predict the torsional resistance of suction caisson with anti-rotation fins in clay. Mar. Struct. 75, 102866.

Gaudin, C., O'Loughlin, C., Duong, T., Herduin, M., Fiumana, N., Draper, S., Wolgamot, H., Zhao, L., Cassidy, M., 2018. New anchoring paradigms for floating renewables. In: Proceedings of the 12th European Wave and Tidal Energy Conference, United Kingdom, p. 9.

Gourvenec, S., 2008. Effect of embedment on the undrained capacity of shallow foundations under general loading. Geotechnique 58 (3), 177–185.

Gourvenec, S., Barnett, S., 2011. Undrained failure envelope for skirted foundations under general loading. Geotechnique 61 (3), 263–270.

Gourvenec, S., Randolph, M., 2003. Effect of strength non-homogeneity on the shape of failure envelopes for combined loading of strip and circular foundations on clay. Geotechnique 53 (6), 575–586.

Gourvenec, S., Randolph, M.F., 2010. Consolidation beneath circular skirted foundations. Int. J. GeoMech. 10 (1), 22–29.

Gourvenec, S.M., Vulpe, C., Murthy, T.G., 2014. A method for predicting the consolidated undrained bearing capacity of shallow foundations. Geotechnique 64 (3), 215–225.

Herduin, M., Gaudin, C., Johanning, L., 2018. Anchor Sharing in Sands: Centrifuge Modelling and Soil Element Testing to Characterise Multi-Directional Loadings.

Hung, L.C., Kim, S.R., 2012. Evaluation of vertical and horizontal bearing capacities ofbucket foundations in clay. Ocean Eng. 52, 75–82.

Li, S., Wang, Y., Li, Q., Huang, J., Li, J., 2019. Failure envelopes of bucket foundations for offshore wind turbines under combined loading including torsion. KSCE J. Civ. Eng. 23 (12), 5154–5162.

Liu, T., Zhang, Y., Meng, Q., 2023. Numerical investigation and design of suction caisson for On-Bottom pipelines under combined V-H-M-T loading in normal consolidated clay. Ocean. Eng. 274, 113997.

Newlin, J.A., 2012. Suction Anchor Piles for the Na Kika FDS Mooring System Part 2: Installation Performance, pp. 55–75.

Nouri, H., Biscontin, G., Aubeny, C.P., 2014. Undrained sliding resistance of shallow foundations subject to torsion. J. Geotech. Geoenviron. Eng. 140 (8), 4014042.

Randolph, M.F., Gaudin, C., Gourvenec, S.M., White, D.J., Boylan, N., Cassidy, M.J., 2011. Recent advances in offshore geotechnics for deep water oil and gas developments. Ocean. Eng. 38 (7), 818–834.

Randolph, M.F., Gourvenec, S.M., 2011. Offshore Geotechnical Engineering. Taylor and Francis, London.

Saviano, A., Pisanò, F., 2017. Effects of misalignment on the undrained HV capacity of suction anchors in clay. Ocean. Eng. 133, 89–106.

Shen, Z., Bie, S., Guo, L., 2017. Undrained capacity of a surface circular foundation under fully three-dimensional loading. Comput. Geotech. 92, 57–67.

Stanier, S.A., White, D.J., 2019. Enhancement of bearing capacity from consolidation: due to changing strength or failure mechanism? Geotechnique 69 (2), 166–173.

Steward, D.P., 1992. Lateral Loading of Piled Bridge Abutments due to Embankment Construction. University of Western Australia.

Suryasentana, S.K., Dunne, H.P., Martin, C.M., Burd, H.J., Byrne, B.W., Shonberg, A., 2020. Assessment of numerical procedures for determining shallow foundation failure envelopes. Geotechnique 70 (1), 60–70.

Suryasentana, S.K., Burd, H.J., Byrne, B.W., Shonberg, A., 2024. Investigation of local soil resistance on suction caissons at capacity in undrained clay under combined loading. Comput. Geotech. 169, 106241.

Taiebat, H.A., Carter, J.P., 2005. A failure surface for caisson foundations in undrained soils. Frontiers in offshore geotechnics. ISFOG 2005 - Proceedings of the 1st International Symposium on Frontiers in Offshore Geotechnics.

Tan, F.S., 1990. Centrifuge and Theoretical Modelling of Conical Footings on Sand. Cambridge University, Cambridge, UK.

Vulpe, C., 2015. Design method for the undrained capacity of skirted circular foundations under combined loading: effect of deformable soil plug. Geotechnique 65 (8), 669–683.

Vulpe, C., Gourvenec, S., Power, M., 2014. A generalised failure envelope for undrained capacity of circular shallow foundations under general loading. Géotech. Lett. 4 (3), 187–196.

Vulpe, C., Gourvenec, S.M., Cornelius, A.F., 2016. Effect of embedment on consolidated undrained capacity of skirted circular foundations in soft clay under planar loading. Can. Geotech. J. 54 (2), 158–172.

Wroth, C.P., 1984. The interpretation of in situ soil tests. Geotechnique 34 (4), 449–489.

Zdravkovic, L., Potts, D., Jackson, C., 2003. Numerical study of the effect of preloading on undrained bearing capacity. Int. J. GeoMech. 3 (1), 1–10.

Zhang, Y., Fan, S., Li, S., Shen, Z., 2024. Numerical analysis of the post-installation consolidated response of skirted foundations. Comput. Geotech. 166, 105931.